Magnetically driven band shift and metal-insulator transition in spin-orbit-coupled $Sr_3(Ir_{1-x}Ru_x)_2O_7$

Seungjae Song,[1] S. Kim,[2] G. H. Ahn,[1] J. H. Seo,[1] Julian L. Schmehr,[3] Michael Aling,[3] Stephen D. Wilson,[3] Y. K. Kim,[2,4,*] and S. J. Moon[1,†]

[1]*Department of Physics, Hanyang University, Seoul 04763, Republic of Korea*

[2]*Department of Physics, Korea Advanced Institute of Science and Technology, Daejeon 34141, Republic of Korea*

[3]*Materials Department, University of California, Santa Barbara, California 93106, USA*

[4]*Graduate School of Nanoscience and Technology, Korea Advanced Institute of Science and Technology, Daejeon 34141, Republic of Korea*

(Received 10 May 2017; revised manuscript received 20 June 2018; published 9 July 2018)

We report a combined infrared and angle-resolved photoemission study of the electronic response of $Sr_3(Ir_{1-x}Ru_x)_2O_7$ ($x = 0, 0.22, 0.34$). The low-temperature optical conductivities of the three compounds exhibit the characteristic feature of the effective total angular momentum $J_{\rm eff} = 1/2$ antiferromagnetic Mott state. As the temperature increases across the antiferromagnetic ordering temperature T_N, the indirect gap gradually closes whereas the direct gap remains open. In the optical conductivity of $Sr_3(Ir_{0.66}Ru_{0.34})_2O_7$ which shows a thermally driven insulator-metal transition at T_N, a Drude-like response from itinerant carriers is registered in the paramagnetic phase. We observe in angle-resolved photoemission data of $Sr_3(Ir_{0.66}Ru_{0.34})_2O_7$ that the valence band shifts continuously toward the Fermi energy with the weakening of the antiferromagnetic order and crosses the Fermi level in the paramagnetic phase. Our findings demonstrate that the temperature-induced metal-insulator transition of the $Sr_3(Ir_{1-x}Ru_x)_2O_7$ system should be attributed to a magnetically driven band shift.

DOI: 10.1103/PhysRevB.98.035110

I. INTRODUCTION

A discovery of the relativistic Mott state in Sr_2IrO_4 [1,2] suggested that the Mott physics can be applicable in 5*d* transition metal oxides and stimulated extensive studies on the nature of their metal-insulator transitions. While the electromagnetic properties of Sr_2IrO_4 were successfully explained in terms of an effective total angular momentum $J_{\rm eff} = 1/2$ Mott state [1–5], a number of experimental and theoretical studies suggested that its ground state should instead be envisioned as a Slater insulator or as an intermediate phase between the Mott and Slater insulators [6–9]. In the Slater picture, the metal-insulator transition occurs at antiferromagnetic ordering temperature T_N via a continuous opening of the band gap due to the appearance of a magnetic supercell [10]. Pyrochlore iridates $R_2Ir_2O_7$ (R = Nd, Sm, and Eu), which have attracted much attention as potential candidates for realizing correlated topological insulators/semimetals [11–13], exhibit a continuous metal-insulator transition accompanying the onset of antiferromagnetic order [14]. A recent angle-resolved photoemission spectroscopy (ARPES) experiment on $Nd_2Ir_2O_7$ [15] showed a gap opening at T_N with an energy shift of quasiparticle peaks in a fashion similar to the Slater transition. The continuous metal-insulator transitions at T_N in $Cd_2Os_2O_7$ and $NaOsO_3$ were also attributed to the Slater transition in early studies [16–19]. Recently, however, the metal-insulator transitions of the two osmates were revisited and ascribed to the Lifshitz-type transition [20–23]. Density-functional-theory calculations showed that the metal-insulator transitions of $Cd_2Os_2O_7$ [20] and $NaOsO_3$ [21] involved a continuous shift of the bands away from the Fermi level and the resulting vanishing of the Fermi surface with decreasing the temperature across their T_N's, which is similar to a Lifshitz-type transition [24]. An optical spectroscopy experiment of $Cd_2Os_2O_7$ also reported that the evolution of the band-edge absorption and itinerant carrier density across the metal-insulator transition can be explained by vanishing of the Fermi surface due to a continuous band shift [22].

Before realizing many of the proposed novel quantum states in 5*d* transition-metal oxides, it is imperative to first understand the effects of the electronic correlations and the antiferromagnetic order within their underlying metal-insulator transitions. The $Sr_3(Ir_{1-x}Ru_x)_2O_7$ system is ideally suited for addressing this issue. The parent compound $Sr_3Ir_2O_7$ shows the characteristic electronic response of the $J_{\rm eff} = 1/2$ antiferromagnetic Mott insulator [3,25], similar to Sr_2IrO_4. However, the small charge gap of about 100 meV [26,27], which is comparable to the magnitude of exchange interaction [28], suggests that $Sr_3Ir_2O_7$ may be in the weak Mott limit [29,30]. Ru doping gradually suppresses the antiferromagnetic order and leads to an insulator-metal transition at a critical Ru concentration $x_c = 0.35$ [25]. On the other hand, the resistivity data $\rho(T)$ of $Sr_3(Ir_{1-x}Ru_x)_2O_7$ compounds in the insulating regime, $x < 0.35$, display a distinct anomaly at T_N, which is not seen in Sr_2IrO_4 systems [31,32]. In particular, for $x \approx 0.33$, the resistivity data show a thermally driven metal-insulator transition at T_N, i.e., $(d\rho/dT > 0)$ at $T > T_N$ and $(d\rho/dT > 0)$ at $T < T_N$, indicating a strong coupling between spin and charge degrees of freedom in the $Sr_3(Ir_{1-x}Ru_x)_2O_7$ system [25,33].

*yeongkwan@kaist.ac.kr
†soonjmoon@hanyang.ac.kr

In this paper, we investigate electronic response of $Sr_3(Ir_{1-x}Ru_x)_2O_7$ ($x = 0$, 0.22, 0.34) by using infrared and angle-resolved photoemission spectroscopies. We show that temperature evolution of the electronic response of $Sr_3(Ir_{1-x}Ru_x)_2O_7$ should be attributed to a continuous band shift, similar to the case of Lifshitz-type transition. The temperature variations of the infrared data involves a redistribution of the optical spectral weight and resulting collapse of the optical gap at $T > T_N$. Absorption edge data reveal distinct temperature variations of the indirect and direct gaps; whereas the indirect gap closes at T_N, the direct gap remains open. Parallel ARPES data of $Sr_3(Ir_{0.66}Ru_{0.34})_2O_7$, which shows a thermally induced metal-insulator transition, identify that the valence band near the X point shifts toward the Fermi energy with increasing the temperature across T_N. In the paramagnetic phase, the valence band crosses the Fermi level, leading to the emergence of the Fermi surface. Our spectroscopic data demonstrate that the antiferromagnetism plays a decisive role for the thermally driven insulator-metal transition in the spin-orbit-coupled Mott system $Sr_3(Ir_{1-x}Ru_x)_2O_7$.

II. RESUTLS AND DISCUSSION

Figure 1 shows the real part of the optical conductivity $\sigma_1(\omega)$ spectra of $Sr_3(Ir_{1-x}Ru_x)_2O_7$. Detailed information on the experiments is given in Supplemental Material [34]. Before discussing the temperature dependence, we summarize the doping evolution of the electronic structure of the ground state, which can be inferred from $\sigma_1(\omega)$ at 10 K. The conductivity data of $Sr_3Ir_2O_7$ can be explained in terms of the $J_{\rm eff} = 1/2$ picture [1,3,35]; the peaks labeled as α and β can be attributed to the optical transitions from the $J_{\rm eff} = 1/2$ lower Hubbard band to the $J_{\rm eff} = 1/2$ upper Hubbard band and from the $J_{\rm eff} = 3/2$ bands to the $J_{\rm eff} = 1/2$ upper Hubbard band, respectively. A sizable amount of Ru substitution of 22% appears to induce minimal changes, and the spectral shape of $\sigma_1(\omega)$ of $Sr_3(Ir_{0.78}Ru_{0.22})_2O_7$ at 10 K is nearly the same as that of $Sr_3Ir_2O_7$ except for an overall increase in the conductivity. Whereas further Ru doping of 34% induces the emergence of an in-gap excitation (peak I) in the energy region below 0.3 eV, the electronic ground state remains barely insulating. The appearance of the in-gap excitation indicates the doping of localized charge carriers [36], most likely localized holes, to the system because Ru^{4+} and Ir^{4+} ions have four $4d$ and five $5d$ electrons, respectively. This combined response suggests that the electronic correlations may play an important role to forbid the doped carriers at the Ru^{4+} ($4d^4$) to transfer to the neighboring Ir^{4+} site ($5d^5$), as observed in a scanning tunneling spectroscopy study [25].

Having established the doping-induced changes in the electronic structure of the ground state, the conductivity data in Fig. 1 also show strong temperature dependences, which involve redistribution of spectral weight. The temperature dependence of $\sigma_1(\omega)$ of $Sr_3Ir_2O_7$ and $Sr_3(Ir_{0.78}Ru_{0.22})_2O_7$ are qualitatively the same. As the temperature increases, the conductivity above 0.3 eV is depressed and the spectral weight is shifted to lower energies [Figs. 1(a) and 1(b)]. This leads to the collapse of the optical gap and the suppression of the peaks α and β. Although the observed changes might be explained in terms of the enhancement of the phonon-assisted optical excitation at high temperatures [26], it should be pointed out that the changes in $\sigma_1(\omega)$ of the two compounds are strongest in distinct temperature regions: 265 K $< T <$ 295 K for $Sr_3Ir_2O_7$ and 190 K $< T <$ 230 K for $Sr_3(Ir_{0.78}Ru_{0.22})_2O_7$.

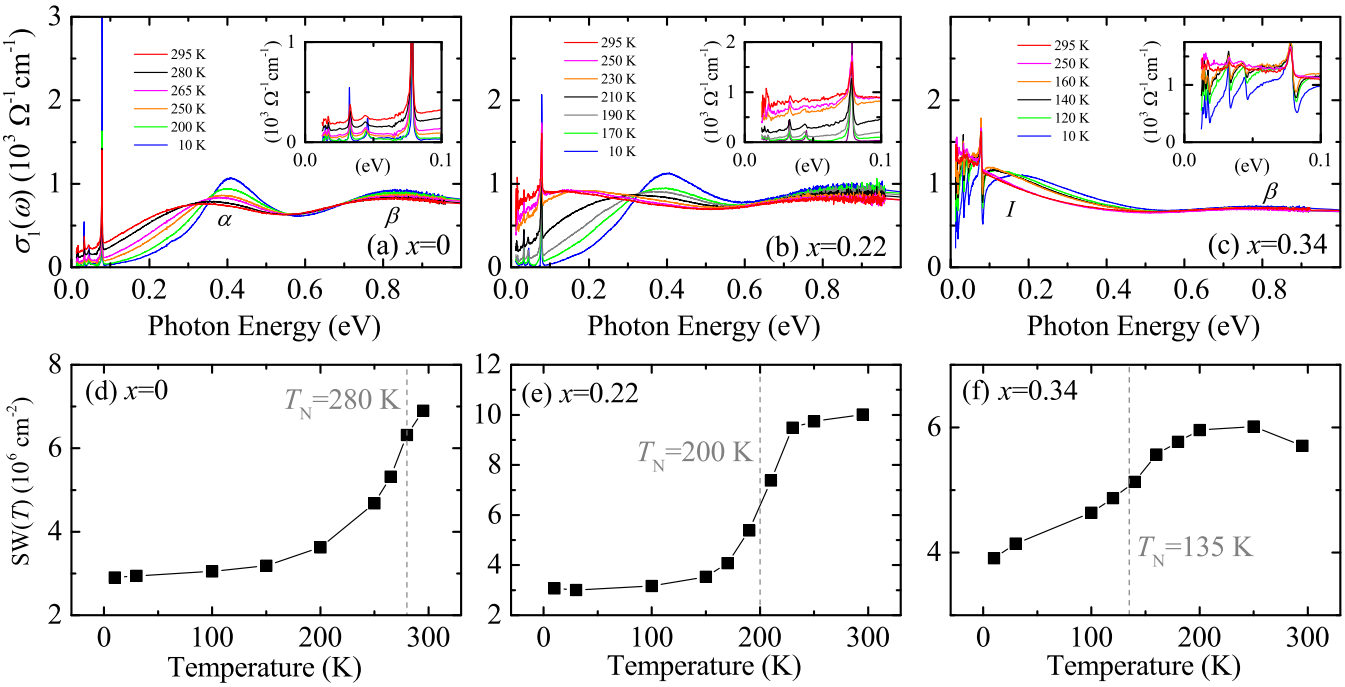

FIG. 1. Optical conductivity spectra $\sigma_1(\omega)$ of $Sr_3(Ir_{1-x}Ru_x)_2O_7$ for (a) $x = 0$, (b) $x = 0.22$, and (c) $x = 0.34$ in the energy region between 0 and 1 eV at selected temperatures. Insets show $\sigma_1(\omega)$ in the far-infrared energy region, i.e., $\omega < 0.1$ eV. Optical SW(ω_c) for (d) $x = 0$ ($\omega_c = 0.35$ eV), (e) $x = 0.22$ ($\omega_c = 0.32$ eV), and (f) $x = 0.34$ ($\omega_c = 0.12$ eV). Dashed lines represent the antiferromagnetic ordering temperatures.

The temperatures at which $\sigma_1(\omega)$ of $Sr_3(Ir_{1-x}Ru_x)_2O_7$ with $x < 0.34$ exhibit the strongest changes are close to their respective T_N's. The $Sr_3(Ir_{1-x}Ru_x)_2O_7$ compounds in the insulating regime, i.e., $x \leqslant 0.34$, show c-axis collinear antiferromagnetic order [25,28]. The T_N's of $Sr_3Ir_2O_7$ and $Sr_3(Ir_{0.78}Ru_{0.22})_2O_7$ are about 280 and 200 K, respectively [25]. At T_N, the resistivity data $\rho(T)$ of $Sr_3(Ir_{1-x}Ru_x)_2O_7$ show a kink, suggesting close coupling between the charge transport and the antiferromagnetic order.

The coupling is most clearly manifested in $Sr_3(Ir_{0.66}Ru_{0.34})_2O_7$, which shows a thermally driven metal-insulator transition at $T_N = 135$ K. The resistivity of $Sr_3(Ir_{0.66}Ru_{0.34})_2O_7$ displays metallic behavior ($d\rho/dT > 0$) at $T > T_N$, while it becomes insulatorlike ($d\rho/dT < 0$) at $T < T_N$ [25]. The optical conductivity data display the spectroscopic signature of the transition observed in the transport measurement [Fig. 1(c)]. As the temperature increases up to 250 K, the spectral weight removed from the energy region above 0.14 eV is shifted to lower energies, leading to the appearance of a Drude-like peak. With further increasing the temperature from 250 to 295 K, $\sigma_1(\omega)$ below (above) about 0.24 eV is slightly suppressed (enhanced), corresponding to the broadening of the Drude-like peak. The far-infrared conductivity at 295 K displays a flat spectral shape, indicating a bad metallic character.

For a more quantitative discussion, we calculate optical spectral weight (SW):

$$\mathrm{SW}(\omega_c) = \int_0^{\omega_c} \sigma_1(\omega) d\omega, \tag{1}$$

where ω_c denotes a cutoff frequency of the integral. We find that the sum rule is satisfied at about 1.5 eV, indicating that the Ir/Ru d states located near the Fermi energy are responsible for the temperature dependence of $\sigma_1(\omega)$ [34]. In order to quantify the changes in the electronic response with the temperature, we choose the isosbestic points in $\sigma_1(\omega)$ of $Sr_3(Ir_{1-x}Ru_x)_2O_7$ as $\omega_c : \omega_c = 0.35$ eV for $Sr_3Ir_2O_7$, $\omega_c = 0.32$ eV for $Sr_3(Ir_{0.78}Ru_{0.22})_2O_7$, $\omega_c = 0.12$ eV for $Sr_3(Ir_{0.66}Ru_{0.34})_2O_7$.

Our spectral weight analysis highlights a crucial role of the antiferromagnetic order for the temperature evolution of the electronic response. Figures 1(d)–1(f) show the temperature dependence of the $\mathrm{SW}(\omega_c)$ of the $Sr_3(Ir_{1-x}Ru_x)_2O_7$ system. It is evident that the change in the $\mathrm{SW}(\omega_c)$ is strongest at T_N. We note that the $\mathrm{SW}(\omega_c)$ of $Sr_3Ir_2O_7$ in the temperature region between 10 and 400 K, which is calculated from $\sigma_1(\omega)$ data in Ref. [26] by using the same protocol, also exhibits the trend of the rapid change across T_N (not shown). The evolution of the electronic response with the temperature cannot be attributed to structural transition. The end members of the

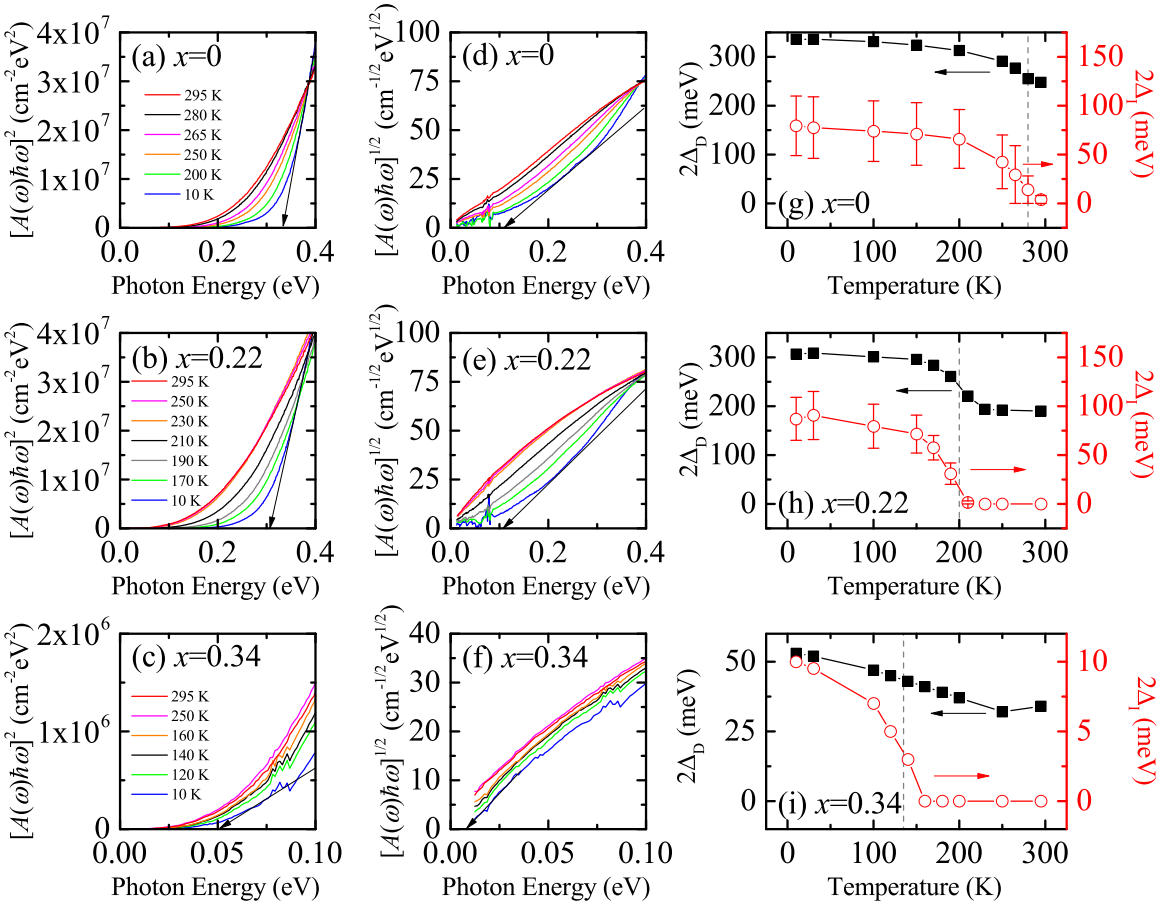

FIG. 2. $[A(\omega)\hbar\omega]^2$ and $[A(\omega)\hbar\omega]^{1/2}$ spectra at selected temperatures where $A(\omega)$ is absorption coefficient: (a), (d) $x = 0$; (b), (e) $x = 0.22$; (c), (f) $x = 0.34$. The arrows represent the tangential line at inflection points of the spectra at 10 K. (g)–(i) Temperature variations in the magnitude of the direct and the indirect gaps ($2\Delta_D$ and $2\Delta_I$). Dashed lines represent the antiferromagnetic ordering temperatures.

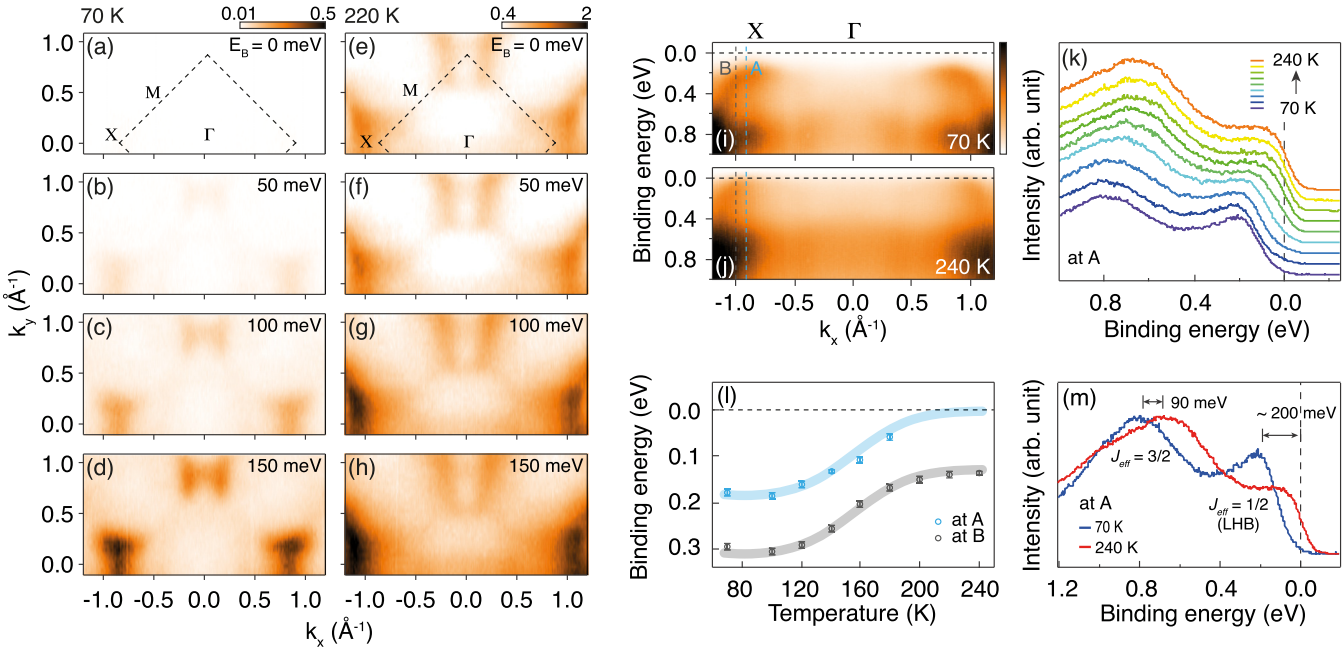

FIG. 3. (a)–(d) Constant energy contour of $Sr_3(Ir_{0.66}Ru_{0.34})_2O_7$ at 70 K. (e)–(h) Constant energy contour at 220 K. The data are, respectively, taken at binding energy $E_B = 0$, 50, 100, and 150 meV. Black dashed lines in (a) and (e) represent Brillouin zone. Band dispersion along Γ-X direction at 70 K (i) and 240 K (j). (k) Photoemission spectra taken at point A [blue dashed line in (i) and (j)]. (l) Temperature-dependent peak energies of the lower Hubbard band obtained at points A and B indicated in (i) and (j). The energies are extracted from fitting of the energy distribution curves (Fig. S2 of Supplemental Material). Thick lines are guides for the eye. (m) Photoemission spectra at point A over broad energy down to -1.2 eV.

system, i.e., $Sr_3Ir_2O_7$ and $Sr_3Ru_2O_7$, do not show any structural transition with the variation in the temperature [37,38]. Further our infrared-active phonon data of $Sr_3(Ir_{1-x}Ru_x)_2O_7$ exhibit gradual changes in the resonance frequencies and the linewidth without any appearance of additional phonon modes.

The redistribution of the spectral weight is associated with variations of the optical gaps. The direct and indirect gaps can be extracted from absorption coefficient $A(\omega)$ [39–42]:

$$A(\omega)\hbar\omega \propto (\hbar\omega - 2\Delta_D)^{1/2}, \tag{2}$$

$$A(\omega)\hbar\omega \propto (\hbar\omega - 2\Delta_I \mp \hbar\omega_{ph})^2. \tag{3}$$

$2\Delta_D$ and $2\Delta_I$ are the direct and indirect gaps, respectively. $\hbar\omega_{ph}$ represents the phonon energy which is involved in indirect transitions, with the $-$ sign corresponding to the phonon absorption process and the $+$ sign to the phonon emission process. Figures 2(a)–2(f) show temperature-dependent $[A(\omega)\hbar\omega]^2$ and $[A(\omega)\hbar\omega]^{1/2}$ of $Sr_3(Ir_{1-x}Ru_x)_2O_7$. We estimated $2\Delta_D$ and $2\Delta_I$ by taking the crossing point of the tangential line at the inflection point of the $[A(\omega)\hbar\omega]^2$ and $[A(\omega)\hbar\omega]^{1/2}$ with the abscissa, respectively.

The analysis of the optical gaps demonstrates interdependence between the optical gaps and the antiferromagnetic order. We find that the $2\Delta_I$ of the $Sr_3(Ir_{1-x}Ru_x)_2O_7$ compounds closes at T_N. The $2\Delta_D$ decreases rapidly at T_N yet remains open at all measurement temperatures. We emphasize that this latter behavior cannot be explained in terms of the Slater mechanism, which should involve an opening of the band gap due to an emergence of a magnetic supercell [10]. In $Sr_3(Ir_{1-x}Ru_x)_2O_7$, the magnetic unit cell is the same as the lattice unit cell and the band folding due to the antiferromagnetic order would not be viable [28,29,43–45], which is confirmed by our ARPES data shown in Fig. 3. Indeed, the staggered rotation of the IrO_6 octahedra breaks the translational symmetry and leads to the opening of the direct gap in cooperation with the electronic correlations [30].

The temperature evolution of the electronic response revealed in our data can be attributed to a magnetically driven band shift [24] with the suppression of the antiferromagnetic order and the resulting emergence of the Fermi surface. According to the band-structure calculations, the conduction-band minimum and the valence-band maximum of $Sr_3Ir_2O_7$ were located near the M and X points in the tetragonal Brillouin zone, respectively [46–49]. They are away from the Fermi energy by a few hundred meV or less at low temperatures. While the direct gap is related to vertical optical transition, the indirect gap is associated with the optical transition from the valence-band maximum near the X point to the conduction-band minimum near the M point. With the suppression of antiferromagnetic order, the bands can approach the Fermi level gradually [20,21,30]. Depending on the energy separations between the conduction-band minimum/the valence-band maximum and the Fermi energy, one of them may touch the Fermi level to induce finite optical conductivity at the zero-frequency limit and to close the indirect gap.

ARPES data of $Sr_3(Ir_{0.66}Ru_{0.34})_2O_7$ packed in Fig. 3 demonstrate that the change in the electronic structure across T_N is associated with the continuous band shift and the resulting appearance of Fermi surface. Figures 3(a)–3(d) and 3(e)–3(h) show constant energy contours at binding energies $E_B = 0$,

50, 100, 150 meV in the antiferromagnetic ($T = 70$ K) and the paramagnetic ($T = 220$ K) states, respectively. In the antiferromagnetic state, the photoemission intensity at $E_B = 0$ is almost zero and appreciable intensity can be detected only at $E_B > 100$ meV. In sharp contrast, a clear intensity is registered at $E_B = 0$ near the X point in the paramagnetic state. The band dispersions along the Γ-X high-symmetry direction taken at the temperatures below and above T_N in Figs. 3(i) and 3(j) as well as the temperature-dependent photoemission intensity in Fig. 3(k) reveal that the band around the X point shifts upward and crosses the Fermi level as the temperature increases. In order to estimate the temperature evolution of the band shift, we fit the photoemission data at the points A and B indicated in Figs. 3(i) and 3(j) [34]. The peak energy of the lower Hubbard band as a function of temperature shown in Fig. 3(l) highlights that the band shift occurs transiently across T_N with full saturation of the peak energy at both low and high-temperature ends, implying the critical role of the antiferromagnetic order.

The ARPES data further reveal that the shift is not a simple rigid band shift but involves important variation in band dispersion. The comparison between the constant energy maps taken at $E_B = 150$ meV in the antiferromagnetic state [Fig. 3(d)] and that taken at $E_B = 0$ meV in the paramagnetic state [Fig. 3(e)] shows that overall topology of the valence bands changes across T_N as can be seen from the emergence of the spectral weight around the M point at $T > T_N$. At the M point, an electron pocket should be present due to the band shift, which is invisible in our data possibly due to a high hole-doping level. Instead, a hole band is observed and produces the spectral weight at the M point [34]. The nonrigid nature of the band shift can also be seen in the difference between the shifts of the $J_{eff} = 3/2$ and $J_{eff} = 1/2$ bands. Figure 3(m) shows that the $J_{eff} = 3/2$ band shifts upward by about 90 meV but the $J_{eff} = 1/2$ band moves by more than 200 meV. The modification of the relative band dispersion may be associated with the change in the hopping strength upon increasing the temperature across T_N as the system moves toward the paramagnetic metallic state from the antiferromagnetic Mott insulating state. Finally, we note that no clear quasiparticle peak is observed at high temperature, implying a bad metallic character. This latter observation is consistent with the flat spectral shape of the far-infrared conductivity of $Sr_3(Ir_{0.66}Ru_{0.34})_2O_7$ at high temperatures [inset of Fig. 1(d)].

III. SUMMARY

We investigated the electronic response of $Sr_3(Ir_{1-x}Ru_x)_2O_7$ single crystals ($x = 0, 0.22, 0.34$) by using infrared and angle-resolved photoemission spectroscopies. The optical conductivity of the $Sr_3(Ir_{1-x}Ru_x)_2O_7$ compounds exhibits a redistribution of the optical spectral weight and an associated collapse of the optical gap with increasing the temperature. Sum rule analysis shows that this change in the electronic response is strongest at T_N, and our data further reveal that the indirect gap closes at T_N as the low-energy conductivity from itinerant carriers emerge while the direct gap remains open at all measurement temperatures. Angle-resolved photoemission spectroscopy experiments illustrate that a continuous shift of the bands toward the Fermi level with the suppression of the antiferromagnetic order leads to the emergence of spectral weight at the Fermi level in $Sr_3(Ir_{0.66}Ru_{0.34})_2O_7$. Our data conclusively demonstrate that the magnetically driven band shift and the resulting emergence of the Fermi surface is responsible for the temperature evolution of the electronic response in the $Sr_3(Ir_{1-x}Ru_x)_2O_7$ systems.

ACKNOWLEDGMENTS

This research was supported by Basic Science Research Program through the National Research Foundation of Korea (NRF) funded by the Ministry of Science, ICT and Future Planning (Grant No. 2017R1A2B4009413). The work at KAIST is supported by Grants No. NRF-2017R1D1A1B03033537 and No. NRF-2017R1A4A1015426. This work was supported by NSF Award No. DMR-1505549 (S. D. Wilson), as well as by the W. M. Keck Foundation (J.L.S. and M.A.). Part of this study has been performed by using facilities at IBS Center for Correlated Electron systems, Seoul National University, Korea.

S.S. and S.K. contributed equally to this work.

[1] B. J. Kim *et al.*, Phys. Rev. Lett. **101**, 076402 (2008).
[2] B. J. Kim, H. Ohsumi, T. Komesu, S. Sakai, T. Morita, H. Takagi, and T. Arima, Science **323**, 1329 (2009).
[3] S. J. Moon *et al.*, Phys. Rev. Lett. **101**, 226402 (2008).
[4] J. Kim *et al.*, Phys. Rev. Lett. **108**, 177003 (2012).
[5] Y. K. Kim, N. H. Sung, J. D. Denlinger, and B. J. Kim, Nat. Phys. **12**, 37 (2016).
[6] R. Arita, J. Kuneš, A. V. Kozhevnikov, A. G. Eguiluz, and M. Imada, Phys. Rev. Lett. **108**, 086403 (2012).
[7] H. Watanabe, T. Shirakawa, and S. Yunoki, Phys. Rev. B **89**, 165115 (2014).
[8] D. Hsieh, F. Mahmood, D. H. Torchinsky, G. Cao, and N. Gedik, Phys. Rev. B **86**, 035128 (2012).
[9] Q. Li *et al.*, Sci. Rep. **3**, 3073 (2013).
[10] J. C. Slater, Phys. Rev. **82**, 538 (1951).
[11] X. Wan, A. M. Turner, A. Vishwanath, and S. Y. Savrasov, Phys. Rev. B **83**, 205101 (2011).
[12] D. Pesin and L. Balents, Nat. Phys. **6**, 376 (2010).
[13] W. Witczak-Krempa, G. Chen, Y. B. Kim, and L. Balents, Annu. Rev. Condens. Matter Phys. **5**, 57 (2014).
[14] K. Matsuhira, M. Wakeshima, R. Nakanishi, T. Yamada, A. Nakamura, W. Kawano, S. Takagi, and Y. Hinatsu, J. Phys. Soc. Jpn. **76**, 043706 (2007).
[15] M. Nakayama *et al.*, Phys. Rev. Lett. **117**, 056403 (2016).
[16] D. Mandrus, J. R. Thompson, R. Gaal, L. Forro, J. C. Bryan, B. C. Chakoumakos, L. M. Woods, B. C. Sales, R. S. Fishman, and V. Keppens, Phys. Rev. B **63**, 195104 (2001).
[17] W. J. Padilla, D. Mandrus, and D. N. Basov, Phys. Rev. B **66**, 035120 (2002).
[18] S. Calder *et al.*, Phys. Rev. Lett. **108**, 257209 (2012).
[19] I. L. Vecchio, A. Perucchi, P. Di Pietro, O. Limaj, U. Schade, Y. Sun, M. Arai, K. Yamaura, and S. Lupi, Sci. Rep. **3**, 2990 (2013).

[20] H. Shinaoka, T. Miyake, and S. Ishibashi, Phys. Rev. Lett. **108**, 247204 (2012).
[21] B. Kim, P. Liu, Z. Ergönenc, A. Toschi, S. Khmelevskyi, and C. Franchini, Phys. Rev. B **94**, 241113 (2016).
[22] C. H. Sohn *et al.*, Phys. Rev. Lett. **115**, 266402 (2015).
[23] Z. Hiroi, J. Yamaura, T. Hirose, I. Nagashima, and Y. Okamoto, APL Mater. **3**, 041501 (2015).
[24] I. M. Lifshitz, Sov. Phys. JETP **11**, 1130 (1960).
[25] C. Dhital *et al.*, Nat. Commun. **5**, 3377 (2014).
[26] H. J. Park, C. H. Sohn, D. W. Jeong, G. Cao, K. W. Kim, S. J. Moon, H. Jin, D.-Y. Cho, and T. W. Noh, Phys. Rev. B **89**, 155115 (2014).
[27] Y. Okada *et al.*, Nat Mater **12**, 707 (2013).
[28] J. Kim, A. H. Said, D. Casa, M. H. Upton, T. Gog, M. Daghofer, G. Jackeli, J. van den Brink, G. Khaliullin, and B. J. Kim, Phys. Rev. Lett. **109**, 157402 (2012).
[29] S. Fujiyama, K. Ohashi, H. Ohsumi, K. Sugimoto, T. Takayama, T. Komesu, M. Takata, T. Arima, and H. Takagi, Phys. Rev. B **86**, 174414 (2012).
[30] J.-M. Carter and H.-Y. Kee, Phys. Rev. B **87**, 014433 (2013).
[31] S. J. Yuan, S. Aswartham, J. Terzic, H. Zheng, H. D. Zhao, P. Schlottmann, and G. Cao, Phys. Rev. B **92**, 245103 (2015).
[32] X. Chen *et al.*, Phys. Rev. B **92**, 075125 (2015).
[33] G. Cao, Y. Xin, C. S. Alexander, J. E. Crow, P. Schlottmann, M. K. Crawford, R. L. Harlow, and W. Marshall, Phys. Rev. B **66**, 214412 (2002).
[34] See Supplemental Material at http://link.aps.org/supplemental/10.1103/PhysRevB.98.035110 for raw ARPES, reflectivity, and optical spectral weight data.
[35] H. Jin, H. Jeong, T. Ozaki, and J. Yu, Phys. Rev. B **80**, 075112 (2009).
[36] M. Imada, A. Fujimori, and Y. Tokura, Rev. Mod. Phys. **70**, 1039 (1998).
[37] H. Matsuhata, I. Nagai, Y. Yoshida, S. Hara, S.-i. Ikeda, and N. Shirakawa, J. Solid State Chem. **177**, 3776 (2004).
[38] H. Shaked, J. D. Jorgensen, S. Short, O. Chmaissem, S. I. Ikeda, and Y. Maeno, Phys. Rev. B **62**, 8725 (2000).
[39] M. Fox, *Optical Properties of Solids* (Oxford University Press, New York, 2001).
[40] P. Y. Yu and M. Cardona, *Fundamentals of Semiconductors*, 4th ed. (Springer, New York, 2010).
[41] F. Wooten, *Optical Properties of Solids* (Academic, New York, 1972).
[42] E. J. Johnson, Semicond. Semimetals **3**, 153 (1967).
[43] C. Dhital *et al.*, Phys. Rev. B **86**, 100401(R) (2012).
[44] S. Boseggia, R. Springell, H. C. Walker, A. T. Boothroyd, D. Prabhakaran, S. P. Collins, and D. F. McMorrow, J. Phys.: Condens. Matter **24**, 312202 (2012).
[45] J. W. Kim, Y. Choi, J. Kim, J. F. Mitchell, G. Jackeli, M. Daghofer, J. van den Brink, G. Khaliullin, and B. J. Kim, Phys. Rev. Lett. **109**, 037204 (2012).
[46] H. Zhang, K. Haule, and D. Vanderbilt, Phys. Rev. Lett. **111**, 246402 (2013).
[47] B. M. Wojek, M. H. Berntsen, S. Boseggia, A. T. Boothroyd, D. Prabhakaran, D. F. McMorrow, H. M. Rønnow, J. Chang, and O. Tjernberg, J. Phys.: Condens. Matter **24**, 415602 (2012).
[48] J. He *et al.*, Sci. Rep. **5**, 8533 (2015).
[49] P. D. C. King *et al.*, Phys. Rev. B **87**, 241106(R) (2013).